







RESEARCH ARTICLE

10.1029/2022JA030439

The Contribution of Planetary Period Oscillations Toward Circulation and Mass Loss in Saturn's Magnetosphere

O. Agiwal^{1,2} , A. Masters² , G. J. Hunt² , and M. K. Dougherty² 

¹Center for Space Physics, Boston University, Boston, MA, USA, ²Blackett Laboratory, Imperial College London, London, UK

Key Points:

- We show that global periodic oscillations can drive recurrent and long-duration magnetic reconnection in Saturn's magnetosphere
- On year-long timescales, this process may remove upwards of ~20% of the mass loaded into Saturn's magnetosphere by Enceladus
- Under certain conditions, this process may be the dominant driver of global circulation and mass loss within Saturn's magnetosphere

Correspondence to:

O. Agiwal,
oagiwal@bu.edu

Citation:

Agiwal, O., Masters, A., Hunt, G. J., & Dougherty, M. K. (2022). The contribution of planetary period oscillations toward circulation and mass loss in Saturn's magnetosphere. *Journal of Geophysical Research: Space Physics*, 127, e2022JA030439. <https://doi.org/10.1029/2022JA030439>

Received 4 MAR 2022
Accepted 27 MAY 2022

Abstract Magnetic reconnection is a process during which magnetic energy is released as kinetic energy. It is considered a crucial driver of energy transport and mass loss within Saturn's magnetosphere. On long-term timescales, is thought to be predominantly driven by the rapid rotation of equatorially mass-loaded flux tubes (i.e., the Vasyliunas cycle), but there is some non-negligible driving from the solar wind as well (i.e., the Dungey cycle). In this study, we investigate an atmospheric driven phenomenon that modulates Saturn's magnetosphere every ~10.6–10.8 hr, known as planetary period oscillations (PPOs), as an additional driver of magnetic reconnection at Saturn. Using an empirical model of PPO dynamics and Cassini magnetic field and plasma measurements, we find that PPO-driven magnetic reconnection is likely to occur in Saturn's magnetosphere, however, the occurrence of the phenomenon depends on temporally variable characteristics of the PPO systems and spatial asymmetries within Saturn's equatorial magnetosphere. Thus, it is not expected to be an on-going process. On year-long timescales, we find that PPOs are expected to be on par with the Dungey Cycle in driving circulation within Saturn's magnetosphere. However, on ~1–2 weeks-long timescales, under specific conditions where PPO-driven reconnection is expected to be active, this phenomenon can become more significant than the Vasyliunas cycle, and thus dominate circulation within Saturn's magnetosphere. On year-long timescales, this process is estimated to remove upwards of ~20% of the mass loaded into the magnetosphere by Enceladus.

1. Introduction

Saturn's magnetosphere is a dynamic, rapidly rotating, and internally mass-loaded environment (Dougherty, 2006), within which energy circulation and mass loss are thought to be governed by various drivers of a phenomenon known as “magnetic reconnection” (Thomsen, 2013).

Magnetic reconnection is a highly energetic process during which near-antiparallel magnetic field lines undergo topological reconfiguration in the form of “breaking” and “reconnecting” within a sufficiently thin current sheet (Phan et al., 2011). This phenomenon results in stored magnetic energy being released as kinetic energy, and the formation of loop-like structures enclosing magnetic flux and plasma (“plasmoids”) that are removed from the magnetosphere. For the onset of magnetic reconnection to occur, the half-thickness of the current sheet must be on the order of the kinetic length scales (e.g., gyroradius/inertial length) associated with the dominant species in the current sheet (Sanny et al., 1994).

Evidence of both solar wind driven magnetic reconnection (i.e., the Dungey Cycle Dungey, 1963; Fuselier et al., 2014; Huddleston et al., 1997; McAndrews et al., 2008) and reconnection driven by the rapid rotation of equatorially mass-loaded flux tubes (i.e., the Vasyliunas Cycle Vasyliunas, 1983) have been observed at Saturn, which is consistent with the early predictions of Badman and Cowley (2007). The interplanetary magnetic field “reconnects” with Saturn's magnetic field across the dayside magnetopause current sheet, followed by the open lobes of planetary magnetic field lines reconnecting across the (disrupted) midplane current sheet of the magnetotail, during the Dungey cycle. Meanwhile, the Vasyliunas cycle involves reconnection occurring on the radially distended planetary field separated by the equatorial current sheet in the post-dusk local time sector. Arridge et al. (2015), Badman et al. (2015), Badman and Cowley (2007), Jackman et al. (2014), and Masters et al. (2014) have shown that while the Dungey Cycle could be expected to be a significant driver of magnetic reconnection on short-term timescales in Saturn's magnetosphere (i.e., while it is actively occurring), on year-long average timescales, the Vasyliunas Cycle is significantly more dominant.

©2022. The Authors.

This is an open access article under the terms of the [Creative Commons Attribution License](https://creativecommons.org/licenses/by/4.0/), which permits use, distribution and reproduction in any medium, provided the original work is properly cited.

We investigate a phenomenon unique to Saturn known as “planetary period oscillations” (PPOs) as an additional driver of magnetic reconnection within the magnetosphere. PPOs refer to a ~ 10.6 hr oscillation (close to the expected planetary rotation period of ~ 10 hr 33 min [Mankovich et al., 2019]) that are ubiquitously observed in all magnetospheric data sets at Saturn (see Carbary et al., 2012, and references therein) and have been shown to globally modulate the thickness and position of the equatorial current sheet (e.g., Agiwal et al., 2020; Cowley, 2017; Morooka et al., 2009; Provan et al., 2012; Thomsen et al., 2017).

Bradley et al. (2018) and Jackman et al. (2016) have shown a strong correlation between the occurrence of reconnection signatures identified in magnetic field data and intervals where PPO dynamics are expected to thin the equatorial current sheet. Cowley and Provan (2021) have shown that certain signatures of recurrent reconnection every ~ 11 hr identified in Saturn’s magnetosphere by Yao et al. (2018) are also consistent with PPO-driven thinning of the equatorial current sheet. While the correlation between the thinning of the equatorial current sheet and an enhancement in reconnection signatures is intuitive, a direct causation between PPO dynamics and magnetic reconnection has yet to be investigated.

In this study, we use empirical constraints on the PPO systems determined by Agiwal (2021) and Agiwal et al. (2020) to show that PPO dynamics are expected to be able to sufficiently thin the equatorial current sheet to the typical characteristic length scales in certain regions of Saturn’s magnetosphere. Consequently, we evaluate the relative contribution of this phenomenon as compared to the more established drivers of global magnetospheric circulation and mass loss at Saturn.

This paper is laid out as follows: in Section 2, we outline the relevant theory of PPO dynamics and key characteristics of Saturn’s equatorial magnetosphere that allow us to determine the relative occurrence and overall significance of PPO-driven magnetic reconnection. In Section 3, we use empirical constraints on the strength of the PPO systems to show that PPO-driven reconnection is likely to occur in Saturn’s magnetosphere, and discuss the spatial scales and expected occurrence rate of this phenomena. In Section 4, we present estimates for the reconnection voltage and mass loss associated with PPO-driven reconnection and discuss how they compare to the more established drivers of magnetic reconnection at Saturn. In Section 5, we present a summary of our main results and final conclusions.

2. Theory

2.1. Periodic Modulation of the Equatorial Current Sheet

The structure of the magnetic perturbation systems associated with PPOs are relatively well established in literature. For brevity, we will only discuss the aspects of these perturbation systems that are required to understand their role in triggering the onset of magnetic reconnection at Saturn in this section, that is, the thickness modulation of the equatorial current sheet.

The works of Andrews et al. (2008, 2010), Cowley et al. (2017), Espinosa and Dougherty (2000), Espinosa et al. (2003), and Southwood and Kivelson (2007) show that PPOs in Saturn’s magnetosphere are driven by two independently rotating large-scale field-aligned current systems, one in each hemisphere. Observations show that the northern and southern systems have slightly differing rotation periods in the range ~ 10.6 – 10.8 hr, which causes them to drift in and out of phase. Chowdhury et al. (2022) present direct evidence of polar thermospheric winds driving these current systems, confirming previous predictions of ionospheric twin vortices driving these perturbation systems from simulations (Jia & Kivelson, 2012; Kivelson & Jia, 2014; C. G. Smith & Achilleos, 2012) and indirect observations (Hunt et al., 2014).

Each rotating field-aligned current system produces a quasi-uniform perturbation field in the core equatorial region (*within* 10 – $12 R_S$) that closes over the corresponding pole as a quasi-dipolar field (Andrews et al., 2008, 2010; Cowley et al., 2017; Espinosa & Dougherty, 2000; Espinosa et al., 2003; Southwood & Kivelson, 2007). Since the two PPO systems have different rotation periods (Provan et al., 2011) and have been observed to dual-modulate the equatorial magnetosphere (Provan et al., 2012), observations from this region present a “beating” of the two signals which affects the amplitude and phase of the combined signal. The *beat phase* (or, relative phasing) between the two systems is quantified by the parameter $\Delta\Phi$, given by,

$$\Delta\Phi = \Psi_N - \Psi_S, \quad (1)$$

where the PPO phase angle $\Psi_{N,S}$ is an azimuthal angle that can be likened to a longitude system. It indicates the location or “local phase” of the northern (N) and southern (S) PPO systems in the magnetosphere: $\Psi_{N,S} = 0^\circ$ refers to where the quasi-uniform PPO magnetic perturbation fields point radially outwards from the planet in the equatorial region as they rotate within the magnetosphere; $\Psi_{N,S} = 180^\circ$ refers to where they point radially into the planet. The radial perturbation fields have no effect on the planetary field at $\Psi_{N,S} = 90^\circ/270^\circ$, however, this is where the associated field-aligned currents are observed.

When the two PPO systems are in antiphase, that is, the quasi-uniform radial vectors of the northern and southern PPO fields in the equatorial region are antiparallel ($\Delta\Phi = 180^\circ$), thickness modulations of the nightside current sheet are enhanced. When the PPO radial vectors are parallel, that is, the two systems are in phase ($\Delta\Phi = 0^\circ$), thickness modulations are minimized. When the PPO systems are $\pm 90^\circ$ out of phase with each other, that is, in quadrature, the observed thickness modulation is somewhere between in phase and in antiphase behavior.

An illustration showing the dual-modulation of the equatorial current sheet by the two PPO systems while they are in antiphase ($\Delta\Phi = 180^\circ$) is presented in Figure 1, where panels (a–c) each illustrate the dynamics at different PPO phases within one PPO cycle (~ 10.6 hr). These dynamics can trivially be understood by vector addition of the perturbation fields and Saturn's background magnetospheric field. The equatorial quasi-uniform component of each PPO field cancels out and the quasi-dipolar component of each of the PPO fields add, yielding a resultant perturbation field that points either northward or southward. An illustration and description of the global configuration of the PPO perturbation fields and associate current systems can be found in Provan et al. (2018, Figure 1).

Since the planetary magnetic field is orientated southward in Saturn's equatorial magnetosphere, when the resultant PPO perturbation field points northward ($\Psi_N = 0^\circ$, $\Psi_S = 180^\circ$), the planetary dipole is reduced and the current sheet is thinned (e.g., Figure 1a); when the resultant PPO perturbation field points southward ($\Psi_N = 180^\circ$, $\Psi_S = 0^\circ$), the planetary dipole is enhanced which is accompanied by a thicker current sheet (e.g., Figure 1c). At $\Psi_N = 90^\circ/270^\circ$ and $\Psi_S = 270^\circ/90^\circ$; e.g., Figure 1b), the perturbation fields have no effect on the poloidal component of the background field.

An empirical model of the dual PPO modulation of Saturn's equatorial current sheet presented by Cowley et al. (2017) has shown excellent agreement with Cassini magnetic field observations (Agiwal, 2021; Agiwal et al., 2020; Thomsen et al., 2017). While the full model considers both the displacement and thickness modulations of the equatorial current sheet in order to model the PPO modulated magnetic field in Saturn's magnetotail, only the equations associated with the thickness modulation will be discussed in this study.

Cowley et al. (2017) show that the the PPO modulated half-thickness of the current sheet D^* can be determined using,

$$D^* = D - [D_N \cos(\Psi_N) - D_S \cos(\Psi_S)], \quad (2)$$

where D is the half-thickness of the current sheet in the absence of PPO modulation, and $D_{N,S}$ is the amplitude of PPO modulation for each system. Enhancements in thickness modulation are evaluated from Equation 2 when the two PPO systems are in antiphase, with D^* maximizing for $\Psi_N = 0^\circ$ and $\Psi_S = 180^\circ$, and minimizing for $\Psi_N = 180^\circ$ and $\Psi_S = 0^\circ$, which is consistent with the observations of Provan et al. (2012; further discussed in Section 2.2).

The relative strengths of the northern and southern amplitudes in Equation 2 are related by the parameter k , which gives the amplitude ratio of the northern and southern PPO systems:

$$k = \frac{D_N}{D_S}. \quad (3)$$

For $k \gg 1$, the northern PPO system dominates the southern, and vice versa for $k \ll 1$. Andrews et al. (2012) and Provan et al. (2013, 2016, 2018) empirically determine k throughout the Cassini mission, and generally find $k < 1$ to be characteristic during southern solstice at Saturn, and $k > 1$ to be characteristic during northern solstice. For a brief interval following equinox, $k \sim 1$ was determined from observations.

Agiwal (2021) and Agiwal et al. (2020) use magnetic field data, the empirically constrained values of the PPO phases and values of k , and the Cowley et al. (2017) model to determine empirical constraints on the amplitude of PPO modulation $D_{N,S}$ and the thickness of the unperturbed current sheet D for two intervals from the Cassini data

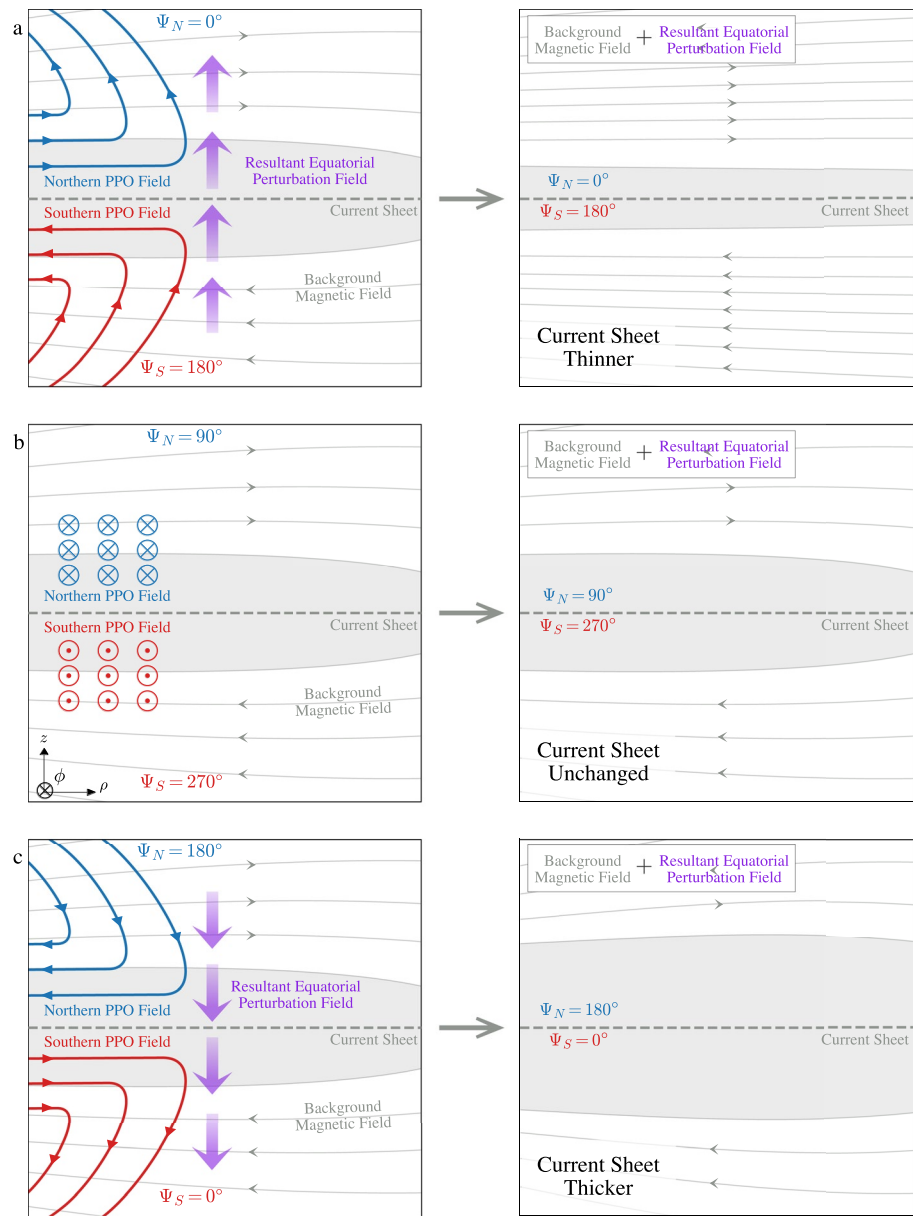


Figure 1. A meridional slice of the magnetosphere is presented in each panel, where we illustrate the dual modulation effect of the northern (blue) and southern (red) planetary period oscillation (PPO) magnetic perturbation fields while they are in antiphase ($\Delta\Phi = 0^\circ$). The perturbation fields are quasi-uniform in the equatorial plane, and close in a quasi-dipolar fashion over the northern and southern poles, respectively, where the planet is to the left of each panel. The equatorial magnetospheric field (internal planetary field + magnetodisc) is illustrated by gray lines and separated by the equatorial current sheet (shaded gray region) and the radial component of the planetary field is positive above the current sheet, and negative below. Simple vector addition of the two PPO fields shows that in panel (a) the resultant PPO perturbation field subtracts from the southward planetary dipole and thus results in a thinning of the current sheet ($D^* < D$ from Equation 2); (b) there is no resultant perturbation field acting on the current sheet ($D^* = D$); (c) the resultant PPO field adds to the southward planetary dipole and thus results in a thicker current sheet ($D^* > D$). The phase angle of the PPO system $\Psi_{N,S}$ ranges between 0° and 360° , where $\Psi_{N,S} = 0^\circ$ is where the quasi-uniform radial PPO vector points directly out from the planet, and $\Psi_{N,S} = 180^\circ$ is where the radial PPO vector points directly into the planet.

set. In Section 3, we use these constraints and Equation 2 to evaluate the PPO modulated half-thickness of the current sheet D^* for an exhaustive range of PPO dynamics. Comparing these results with the characteristic length

scales in Saturn's magnetosphere, that will be discussed in Section 2.2, allows us to determine the likelihood and significance of PPO-driven magnetic reconnection in Saturn's magnetosphere.

2.2. Characteristics of Saturn's Magnetosphere

Saturn's equatorial current sheet is a highly dynamic, azimuthally asymmetric structure, with an inner boundary at $\sim 5\text{--}7 R_S$ ($1 R_S = 60,628$ km; Carbary et al., 2012; Sergis et al., 2018). This structure extends all the way out to the magnetopause boundary at all local times, except at dawn where Staniland et al. (2021) show the occasional existence of a cushion region at Saturn and merges with the magnetotail current sheet in the nightside magnetosphere. It is populated by outgassing from the moon Enceladus (Dougherty, 2006) and predominantly comprised of water group ions (W^+), protons (H^+), and electrons, where the abundance ratio of the two species is $H^+/W^+ \sim 0.7$ (Wilson et al., 2017). The equatorial current sheet acts to radially distend Saturn's planetary field into a "magnetodisc" structure (Arridge et al., 2007; Connerney et al., 1983; thus resulting in a thinner current sheet) beyond $\sim 10\text{--}12 R_S$ at all local times (Sergis et al., 2007, 2009, 2010).

Magnetic field observations have shown the current sheet half-thickness to be temporally variable between ~ 0.7 and $3 R_s$ at noon, and ~ 0.3 and $3 R_s$ at midnight (e.g., Giampieri, 2004; Kellett et al., 2011; Sergis et al., 2011; Staniland et al., 2020), where the temporal variability is attributed to a combination of solar wind compressional effects, PPO modulation, and variable mass-loading from Enceladus. Agiwal (2021) and Agiwal et al. (2020) find the statistical median of the half-thickness of the nightside current sheet in the absence of PPO modulation to be $\sim 1.25 R_S$ from magnetic field data taken near northern solstice, and $\sim 2 R_S$ from an interval near southern solstice.

The midnight and dawn current sheet are on average expected to be thinner than the dusk and noon current sheet (e.g., Agiwal, 2021; Arridge et al., 2015; Delamere et al., 2015; Jia & Kivelson, 2016; Martin & Arridge, 2017; Staniland et al., 2020), although during times of solar wind compression, it is possible that the current sheet may be thinner at dusk than at dawn (Sorba et al., 2019). Staniland et al. (2020) show that the average dayside current sheet may be ~ 2 times thicker than the nightside current sheet beyond $\sim 15 R_S$ in Saturn's magnetosphere. Assuming azimuthal symmetry in the amplitude of PPO modulation between radial distances of $\sim 20\text{--}30 R_S$, we might thus expect PPO-driven magnetic reconnection to be more likely in the nightside magnetosphere/the midnight and dawn local time sectors, where the current sheet is typically expected to be thinner.

As discussed in Section 1, the onset of magnetic reconnection requires the current sheet to be thinner than some characteristic kinetic length scale λ_i associated with the dominant charged particles in the current sheet. Authors such as Biskamp et al. (1997) and Tóth et al. (2017) show that the important length scales are the gyroradius and the inertial length of the charged particles. Most studies do not distinguish between the gyroradius or inertial length of a species when discussing reconnection dynamics, however, Liu et al. (2014, and references therein) provide evidence for the gyroradius of the dominant ion species being more significant than the ion inertial length for reconnection in Earth's magnetotail.

The typical gyroradii and inertial lengths of the dominant ions in Saturn's equatorial current sheet are presented in Figure 2. These length scales were evaluated using plasma moments from CAPS-IMS measurements presented by Wilson et al. (2017). The W^+ ion kinetic length scales $\lambda_i(W^+)$ are much larger than the proton kinetic length scales $\lambda_i(H^+)$ for almost all radial distances presented in Figure 2, and we note that W^+ is the dominant ion species in Saturn's equatorial current sheet. While we cannot be certain if Earth-like conditions would also apply at Saturn, in the absence of other observations, we assume that violating the W^+ ion length scales would make the onset of magnetic reconnection more likely.

A. W. Smith et al. (2016) show that the statistical location of reconnection sites at Saturn is highly variable between $\rho \sim 20$ and $30 R_S$ in the nightside magnetosphere. Thus, we average over the W^+ inertial length and gyroradius between these radial distances at all local times and find an average length scale of $\sim 0.05 R_S$ that we will subsequently use as the threshold length scale that must have to be violated by the thinned current sheet for the onset of magnetic reconnection to become more likely. While we have averaged over local time to evaluate this threshold, the typical ion kinetic length scales presented in Figure 2 are larger in the midnight and dawn local time sectors, than at noon and dusk. The larger ion kinetic length scales in the midnight and dawn local time sectors, combined with the thinner current sheets expected in these sectors further imply that PPO-driven reconnection may be more likely to occur in the midnight and dawn local time sectors.

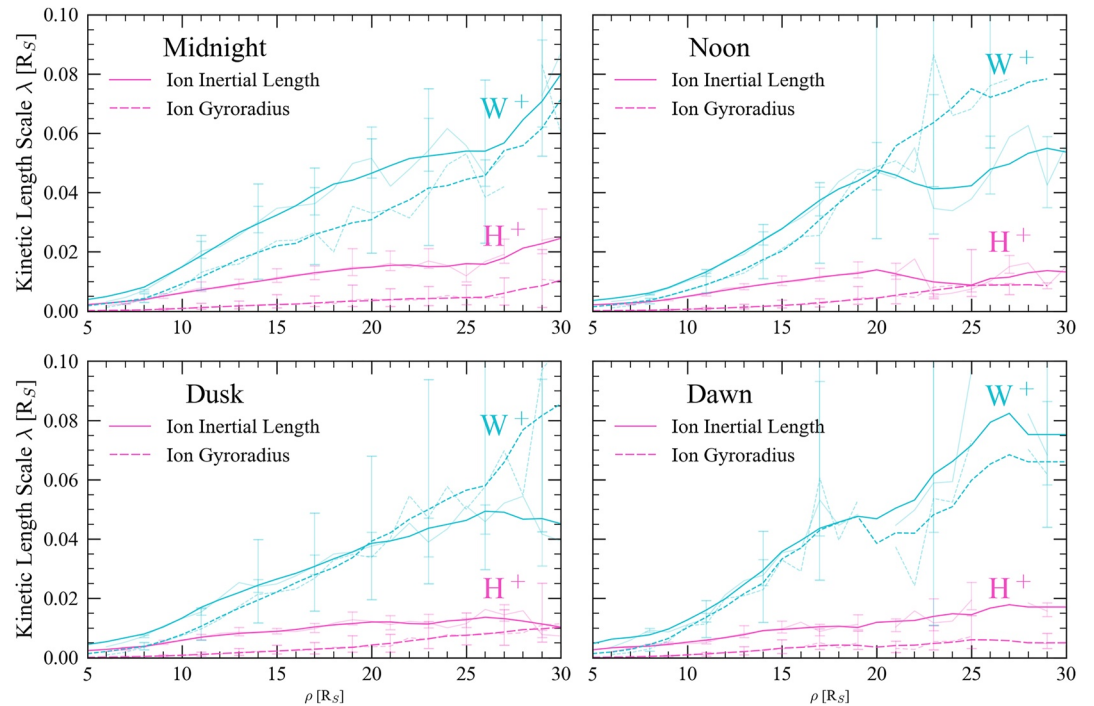


Figure 2. The radial profiles of the characteristic ion inertial lengths (solid lines) and gyroradii (dashed lines) for W^+ (blue) and H^+ (pink) ions are presented for each of the four local time sectors (panels a–d) respectively. The local time quadrants are centered on (a) 00 (b) 12 (c) 18, and (d) 06 hr. These profiles were determined using plasma moments from (Wilson et al., 2017), where the raw profiles calculated with associated error bars are shown as fainter lines in the background, and the solid lines in the foreground are smoothed, averaged profiles. The W^+ ion is the more abundant species in Saturn’s equatorial current sheet, and the associated length scales are much larger than those for H^+ between ~ 20 – $30 R_S$, where the reconnection sites are statistically most likely to form in Saturn’s magnetosphere (A. W. Smith et al., 2016).

2.3. Magnetic Reconnection in Space Plasmas

To determine the contribution of PPO-driven magnetic reconnection toward global circulation within Saturn’s magnetosphere relative to the more established drivers of reconnection, that is, the Dungey and Vasyliunas cycles, we evaluate the “*reconnection voltage*” associated with the proposed mechanism.

The specific area in which magnetic reconnection occurs is referred to as the *diffusion region*, which is a few multiples of the typical ion kinetic length scales λ_i in the current sheet. The magnetic field has an X-like geometry inside the electron diffusion region, where the center of the X-line is a magnetic null point. The reconnecting magnetic field within the diffusion region is thus known as the reconnection X-line.

The inflow of plasma into the magnetic reconnection site maintains a reconnection electric field E , which is tangential to the plasma inflow and reconnecting magnetic field, and assumed to be constant along the length of the X-line l_x (the azimuthal extent of the reconnection site). The potential difference V applied to the magnetosphere due to this E can be determined using,

$$V = l_x E. \quad (4)$$

In the equatorial current sheet, where the magnetic field strength B and the plasma properties are expected to be symmetric on either side of the current sheet center, E can be computed using,

$$E = \kappa B V_{out}, \quad (5)$$

where $\kappa = 0.1$ is the reconnection efficiency determined empirically in the near-Earth solar wind environment. The reconnection efficiency is thought to be dependent on the plasma environment surrounding the reconnection site (e.g., Chen et al., 2017; Nakamura et al., 2018; Slavin & Holzer, 1979), and controls the rate at which magnetic energy is converted to kinetic energy. While this rate can be variable in different plasma environments

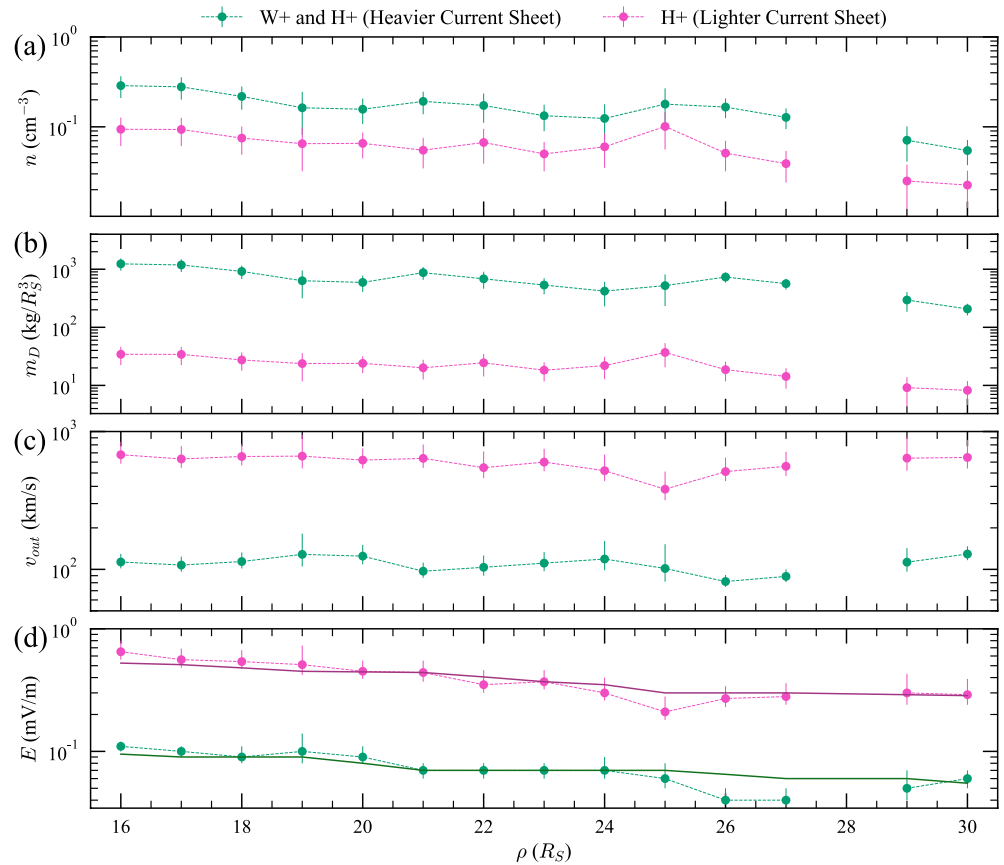


Figure 3. We present the radial profiles of (a) the median ion number densities from (Wilson et al., 2017), (b) the mass density, (c) the ion outflow velocity, and (d) the reconnection electric field. Two profiles are presented in each panel, one depicting a “heavier” current (green) sheet with W^+ and H^+ ions with relative abundance $H^+/W^+ \sim 0.7$ (the nominal mass density of the equatorial current sheet), and one depicting a “lighter” current sheet (pink) with H^+ only (a proxy for a mass-depleted current sheet). The v_{out} and E profiles associated with the lighter current sheet are approximately an order of magnitude larger than the corresponding outputs for a heavier current sheet. In panel (d), smoothed running averages of the electric field profile are shown by solid lines.

(e.g., DiBraccio et al., 2013; Slavin & Holzer, 1979), it is not particularly well constrained elsewhere. Therefore, this nominal value of ~ 0.1 has also been applied to Saturn’s magnetosphere by authors such as Badman and Cowley (2007) and Masters (2015).

The speed at which ions are accelerated away from the reconnection site is given by v_{out} , where the ions move radially away from the reconnection site in the tailward/planetward sense. In the equatorial magnetosphere, v_{out} can be evaluated using,

$$v_{out} = \frac{B}{\sqrt{\mu_0 m_{Di}}}, \quad (6)$$

where B is the magnetic field strength tangential to the reconnection site (i.e., the lobe field strength in the magnetotail), $m_{Di} = \sum m_i n_i$ is the total mass density of the current sheet, where the density is the sum of all the dominant ion species i in the current sheet, and μ_0 is the magnetic permeability of free space.

In Figure 3, we present the radial profiles of (a) the median ion number densities from W17, (b) the mass density, (c) the ion outflow velocity, and (d) the reconnection electric field. Two profiles are presented in each panel, one depicting a “heavier” current sheet with W^+ and H^+ ions with relative abundance $H^+/W^+ \sim 0.7$ (the nominal mass density of the equatorial current sheet), and one depicting a “lighter” current sheet with H^+ only (a proxy for a mass-depleted current sheet). We employ the Jackman and Arridge (2011) empirical model of Saturn’s lobe field strength to evaluate B to calculate v_{out} using Equation 6 and consequently, E using Equation 5. The v_{out}

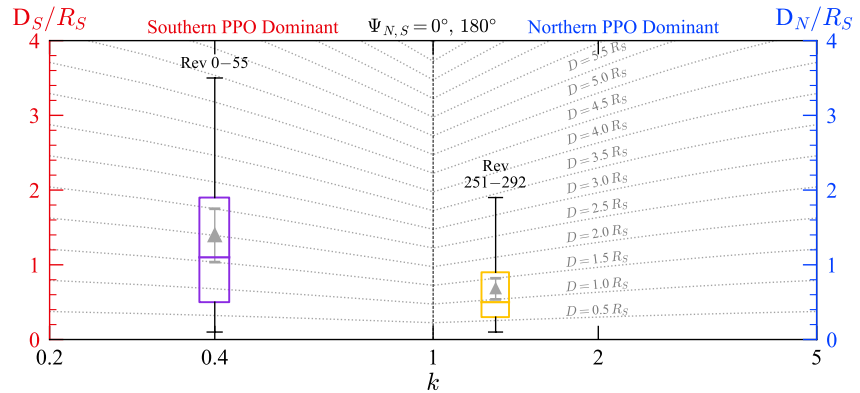


Figure 4. Box-whisker plots indicate empirically constrained distributions of $D_{N,S}$ for two intervals from the Cassini mission: Revs 0–55 (purple, at $k = 0.4$) and Revs 251–292 (yellow, at $k = 1.3$). The box indicates the median and inter-quartile range, while the whiskers indicate the inter-decile range of the distributions. Gray dotted lines indicate the amplitude of $D_{N,S}$ amplitudes required to thin a current sheet with half-thickness D (as indicated on plot) to $D^* \sim 0.05 R_S$ for $k = D_N/D_S$ between 0.2 and 5 when $\Psi_{N,S} = 0^\circ, 180^\circ$, that is, the two planetary period oscillations (PPO) systems are in antiphase and maximum thinning of the current sheet is expected. For $k < 1$ ($k > 1$), the gray dotted lines correspond to the D_S (D_N) axis. At $k = 1$, $D_N = D_S$. For each interval, the median value of D (the current sheet half-thickness in the absence of PPO modulation) constrained by A20/21 is shown by a gray triangle marker placed on the corresponding D isocontour and the associated gray errorbars indicate the inter-quartile range of the distribution.

and E profiles associated with the lighter current sheet are approximately an order of magnitude larger than the corresponding outputs for a heavier current sheet. Provided that PPO dynamics can sufficiently thin the equatorial current sheet to length scales $< 0.05 R_S$, the only parameter that still needs to be computed to determine the reconnection voltage is the length of the reconnection X-line.

While the heavier current sheet profile presented in Figure 3 is representative of typical densities in Saturn's equatorial current sheet, Arridge et al. (2016) identify ions leaving a reconnection site observed at a radial distance of $\sim 30 R_S$ in Saturn's nightside magnetosphere with velocities on the order of $\sim 1,200$ km/s, which are more consistent with the H^+ only current sheet presented in Figure 3. The authors provided evidence of ongoing but time variable reconnection over a ~ 19 hr interval, and thus attributed the higher velocities to a mass-depleted current sheet at the reconnection site, where the water group ions had been expelled downtail. As this study is concerned with a phenomenon that may drive recurrent reconnection, we find it appropriate to consider both the lighter and heavier current sheet approximations in our discussion.

3. Results

Agiwal (2021) and Agiwal et al. (2020) (hereafter A20/21) evaluate empirical constraints on the amplitude of PPO modulation $D_{N,S}$ and current sheet half-thickness in the absence of PPO modulation D . In this section, we will use these parameters to constrain the length of the reconnection X-line formed during PPO-driven reconnection.

A20/21 use Cassini magnetic field data (Dougherty et al., 2004), empirically determined values of k and $\Psi_{N,S}$ determined by (Andrews et al., 2012; Provan et al., 2013, 2016, 2018) throughout the Cassini mission, and the fully resolved Cowley et al. (2017) model to determine empirical constraints on the values of D and $D_{N,S}$ from two intervals in the Cassini data set in the nightside magnetosphere: Revs 0–55 (southern solstice) and Revs 251–292 (northern solstice). These distributions are shown in Figure 4 as box-whisker plots, where the box represents the median and inter-quartile range, and the whiskers represent the inter-decile range, and the amplitudes shown are for the dominant PPO system during that interval, that is, D_S for the southern solstice interval, and D_N for the northern solstice interval. A20/21 show the best-fit amplitude of PPO oscillation $D_{N,S}$ to vary on a Rev-by-Rev basis, where during the northern solstice interval, where Cassini performed its fastest orbits, the amplitudes were observed to be variable on ~ 1 – 2 weeks-long timescales.

Rearranging Equation 2 for $D_{N,S}$ by making the substitution $k = D_N/D_S$ to only solve for D_S when $k < 1$ and D_N when $k > 1$, we can determine the PPO amplitudes required to thin a current sheet with unperturbed half-thickness D to $D^* = 0.05 R_S$, for any given configuration of the PPO systems. We initially investigate the conditions

when the current sheet undergoes maximum thinning, that is, the two PPO systems are perfectly in antiphase $\Delta\Phi = 180^\circ$, and the northern and southern PPO systems are at phase angles $\Psi_{N,S} = 0^\circ, 180^\circ$ respectively. By comparing the evaluated $D_{N,S}$ amplitudes with the $D_{N,S}$ amplitudes constrained by A20/21, we can determine if PPO-driven reconnection is likely to occur in Saturn's magnetosphere.

In Figure 4, we present the $D_{N,S}$ amplitude (D_S for $k < 1$ and D_N for $k > 1$) required to sufficiently thin a current sheet with unperturbed half-thickness D as dotted gray lines, where the D associated with each line is indicated on the plot. The gray triangle markers with error-bars at $k = 0.4$ and $k = 1.3$ indicate the median and inter-quartile range of the distribution of D values constrained by A20/21 from each interval. A20/21 attribute the variability in D to the compression state of the magnetosphere, where thinner current sheets are thought to be associated with a more expanded magnetosphere (e.g., Sorba et al., 2019).

A20/21 find that the data is typically better fit by a thicker current sheet ($D \sim 2 R_S$) during the southern solstice interval than the northern solstice interval ($D \sim 1.25 R_S$). Correspondingly, the D_S amplitudes that fit the data well during the southern solstice interval are on average larger than the D_N amplitudes that best-fit the northern solstice interval. From the $D_{N,S}$ distributions, we see that PPO modulation amplitudes greater than the median are required to thin the a current sheet with median D to length scales of $D^* = 0.05 R_S$ for both intervals. For the northern solstice interval D_N is greater than the median of the distribution for a duration of ~ 1 – 2 weeks every ~ 6 – 8 weeks. For the southern solstice interval, A20/21 were unable to determine an equivalent timescale for when D_S is greater than the median of the distribution due to the events analyzed being more spaced apart in time.

Therefore, even though PPO-driven reconnection can occur in Saturn's magnetosphere, it is not expected to be an ongoing process. Additionally, the similarity in the relative distribution of the $D_{N,S}$ amplitudes that can sufficiently thin the equatorial current sheet between the two intervals analyzed indicates that the likelihood of PPO-driven reconnection may not be significantly variable with Saturnian season.

We now investigate if PPO-driven reconnection can occur at other phase angles in a single PPO cycle, and for non-antiphase beat phase conditions as well, assuming the median D half-thickness values of $\sim 2 R_S$ for the southern solstice interval and $\sim 1.25 R_S$ for the northern solstice interval. For a given PPO beat phase $\Delta\Phi$, the phase angles Ψ_N where Equation 2 yields $D^* < 0.05 R_S$ are then used to constrain the azimuthal extent over which PPO-driven reconnection is favorable. We find that the PPO phase angles that satisfy the aforementioned condition are always sequential, thus returning an "arc" of PPO phases that would be able to trigger the onset of magnetic reconnection as they rotate within the magnetosphere. Such an arc effectively gives us the azimuthal extent of the PPO-driven reconnection site θ_x , which consequently allows us to evaluate the associated reconnection voltage (Section 2.3).

In Figure 5a, we present profiles of the angular extent of the reconnection favorable PPO phases θ_x evaluated assuming the upper-quartile values of $D_S = 1.9 R_S$ for the southern solstice interval (dotted purple line) and $D_N = 0.9 R_S$ for the northern solstice interval (dotted yellow line). As expected, the largest θ_x is evaluated when the two PPO systems are in antiphase ($\Delta\Phi \sim 180^\circ$), with $\theta_x \sim 86^\circ$ and 82° for the southern and northern intervals respectively, where the similarity between the two profiles indicates that the occurrence of PPO-driven reconnection may not be significantly variable with Saturnian season. Across the two intervals presented in Figure 5, we observe that PPO-driven reconnection is only favorable while $\Delta\Phi \sim 180^\circ \pm 90^\circ$.

We have thus far shown that the onset of PPO-driven reconnection is dependent on multiple factors, including: the amplitude of PPO modulation $D_{N,S}$, the beat phase $\Delta\Phi$ between the two PPO systems, and the half-thickness of the equatorial current sheet in the absence of PPO modulation D . In order to understand the significance of this process in driving the magnetosphere compared to the more established drivers of reconnection, we will evaluate an average value of θ_x taking into account the temporal variability of the amplitude and beat phases of the PPO systems.

Thus, for each interval, we evaluate θ_x profiles as a function of PPO beat phase for the full distribution of $D_{N,S}$ amplitudes constrained by A20/21. Using the normalized distribution of $D_{N,S}$ values (presented in Figure 5b) as weightings, we then compute a weighted average θ_x profile for each interval, which are shown solid purple (northern interval) and yellow (southern interval) in Figure 5a. The weighted average θ_x profiles peak at much lower θ_x values than the dotted profiles corresponding to the upper-quartile $D_{N,S}$ values, which shows that the variability in $D_{N,S}$ is equivalent to a shorter X-line forming in the magnetosphere. However, the solid line profiles in Figure 5a

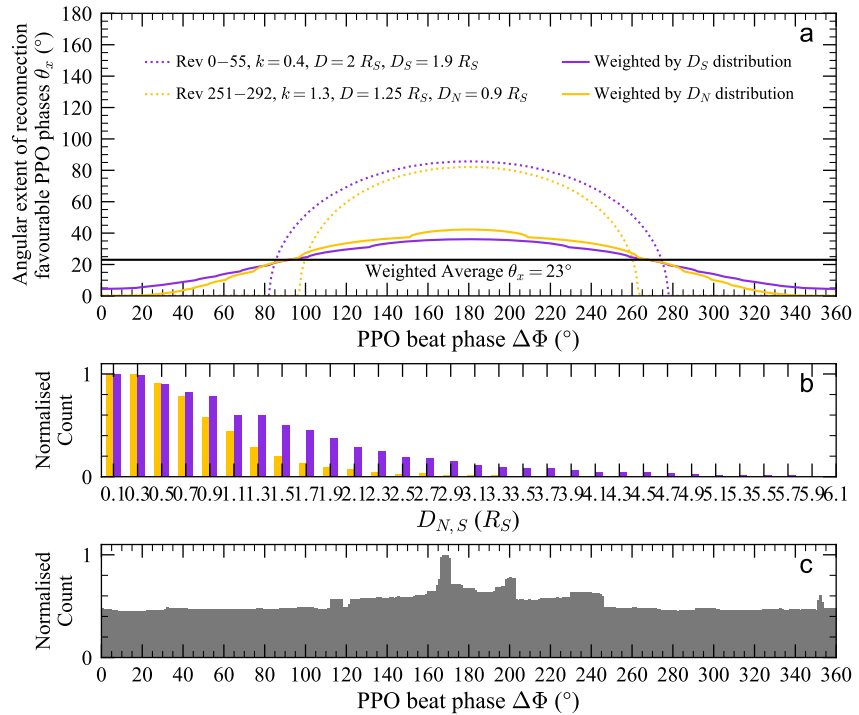


Figure 5. In panel (a), we present the total angular extent of planetary period oscillation (PPO) phases for which reconnection may be favorable, θ_x , as shown as a function of PPO beat phase $\Delta\Phi$ for two intervals from the Cassini data set: Revs 0–55 (purple) and Revs 251–292 (yellow). The empirical constraints on the PPO systems and magnetospheric conditions used to evaluate each profile are indicated on the plot. The dotted lines indicate θ_x calculated using $D_{N,S}$ using the upper-quartiles constrained from A20/21, whereas the solid lines show the average θ_x profile weighted by the empirically constrained $D_{N,S}$ distributions from the same authors, presented in panel (b). The solid yellow and purple lines are then additionally weighted by the empirically constrained $\Delta\Phi$ distributions presented in panel (c), and then averaged to return the solid black line in panel (a), which represents the weighted average θ_x value of 23° that has been temporally averaged for the variability in PPO amplitude, beat phase, and Saturnian season.

also indicate that PPO-driven reconnection may be expected to occur over a much wider range $\Delta\Phi$ values, owing to values of $D_{N,S}$ that are greater than the upper-quartile in the distribution. The weighted average θ_x is non-zero even during perfectly in phase ($\Delta\Phi = 0^\circ$) conditions for the southern solstice profile. This is not entirely unexpected, seeing as the southern PPO system is ~ 2.5 times more dominant than the northern PPO system during this time, and thus the thickness modulation of the current sheet is not expected to fully cancel out in Equation 2.

In order to constrain a θ_x value without any significant dependency on PPO dynamics, we now weight both of the solid line profiles presented in Figure 5a by the normalized distribution of empirically constrained PPO beat phases over the entire Cassini mission presented in Figure 5c (Andrews et al., 2012; Provan et al., 2013, 2016, 2018). Though this distribution is mostly flat, the beat phases close to near anti-phase values have a modestly higher count.

From this calculation, we evaluate the weighted average value of the angular extent of reconnection favorable PPO phases to be $\theta_x \sim 23^\circ$. This value is much smaller than the peak θ_x values considered during active times of PPO driven reconnection, but this shorter X-line that is consistently present in the magnetosphere is a proxy that accounts for the temporal variability of PPO amplitude, PPO beat phase, and Saturnian season.

4. Discussion

4.1. Evaluating the Reconnection Voltage

Using our constraints on the azimuthal extent of the X-line on both short-term (while PPO-driven reconnection is expected to be active) and long-term timescales (>year-long timescales), we now evaluate the reconnection voltages associated with this phenomenon in Saturn's magnetosphere.

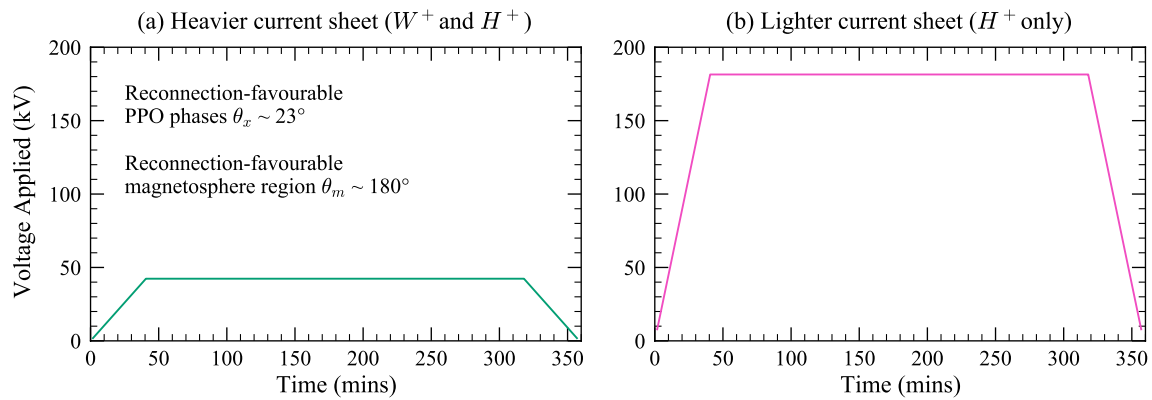


Figure 6. We show the time-evolution of the voltage applied to the magnetosphere for an example X-line with angular extent $\theta_x \sim 40^\circ$ as it rotates through a $\theta_m \sim 180^\circ$ region of the magnetosphere where reconnection is favorable (i.e., D typically thinner). The X-line is assumed to form at radial distance $\rho = 25 R_S$. This voltage is calculated for the limits of (a) a heavier current sheet and (b) a lighter current sheet as described in Figure 3.

In Section 2.2, we discussed that PPO-driven reconnection may be more likely in the midnight and dawn local time sectors, where the current sheet is expected to be thinner and the characteristic kinetic length scales are shown to be larger. Thus, only half, or $\sim 180^\circ$ of the equatorial magnetosphere would have current sheet conditions favorable for PPO-driven reconnection. For our proposed phenomenon to occur in the dusk/noon local time sectors, additional thinning of the current sheet due to non-PPO driving, or local time asymmetries in the strength of the PPO systems would be required, but such behavior is not expected to be “typical” in Saturn’s magnetosphere. Therefore, for the remainder of our discussion, we assume that PPO-driven reconnection might only be triggered while the reconnection favorable PPO phases θ_x are within the midnight and dawn local time sectors. The angular extent of the region where the equatorial current sheet allows for reconnection to be favorable will hereafter be characterized by θ_m .

In Figure 6, we show the time-variable evolution of the reconnection voltage associated with a modeled event, where we assume the azimuthal extent of the reconnection favorable PPO phases to be $\theta_x = 23^\circ$. In our modeled event, this $\sim 23^\circ$ arc of reconnection favorable PPO phases rotates through the midnight and dawn local time sectors, that is, $\theta_m = 180^\circ$. The voltage is evaluated using Equation 4, for a predicted reconnection site at $\rho = 25 R_S$. The time taken for the PPO phases to rotate through 1° of Saturn’s magnetosphere is ~ 1.77 min. Thus, for $\theta_x = 23^\circ$, a time-variable voltage is applied for ~ 38 min at the beginning and end of the event modeled in Figure 6. There is a potential difference applied to Saturn’s magnetosphere for a total of ~ 360 min (~ 6 hr) during our modeled event, and assuming that PPO-driven reconnection can persist over 1–2 weeks-long timescales as inferred by A20/21, this process would then restart ~ 4 hr later. The ~ 6 hr reconnection event modeled in this section is found to be consistent with the results of Reed et al. (2018), who show that ~ 264 short-duration events (< 20 hr) of low frequency extensions in Saturn kilometric radiation, a feature associated with tail reconnection, can typically last up to ~ 8 hr.

Figures 6a and 6b use E associated with the heavier and lighter current sheets presented in Figure 3, where E is variable with radial distance, but constant over time in each panel. The peak voltage applied to the magnetosphere changes drastically depending on the mass-content of the current sheet, where in the heavier current sheet approximation, the predicted voltage peaks at ~ 45 kV, whereas for the lighter current sheet, V peaks at ~ 180 kV. We cannot constrain the extent of mass-depletion without more specific knowledge of each reconnection event, but assume instead that the peak voltage applied to the Saturnian system during the modeled reconnection event lies in the range between ~ 45 kV (heavier current sheet) and 180 kV (lighter current sheet).

The total amount of magnetic flux involved in reconnection during our modeled event can be estimated by integrating the voltage presented in Figure 6 over time. Assuming (a) the heavier current sheet, we evaluate ~ 0.9 GWb of reconnected flux over the ~ 6 hr event, whereas for (b) the lighter current sheet limit, we evaluate ~ 4 GWb of reconnected flux over the same time interval. While reconnection is active, the average voltage applied to the magnetosphere lies in the range between (a) ~ 45 kV and (b) ~ 180 kV. However, on ~ 10.6 hr timescales (1 PPO cycle), reconnection is not expected to occur for ~ 4 hr. Thus, the total voltage applied to the system averaged over one PPO cycle is in the range (a) ~ 25 kV – (b) ~ 100 kV.

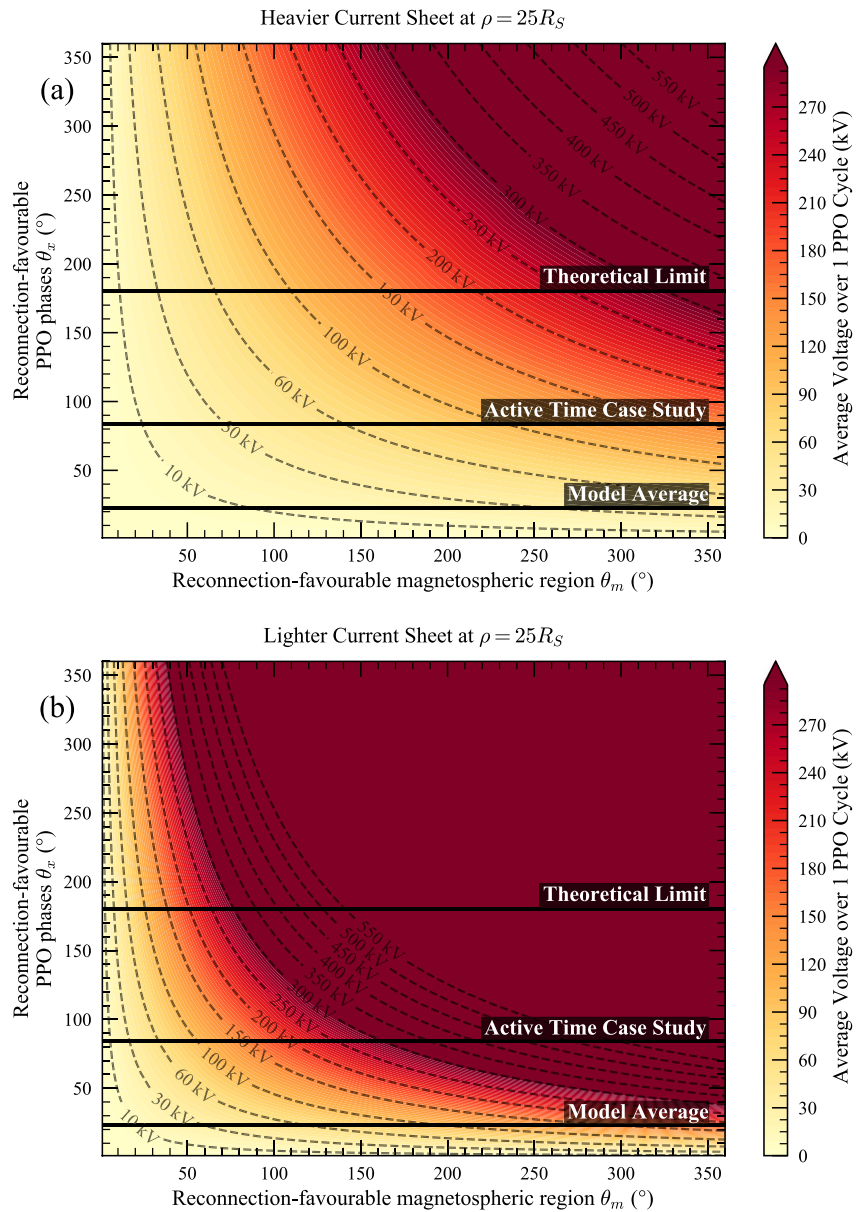


Figure 7. The expected reconnection voltage over 1 planetary period oscillations (PPO) cycle for all iterations of $\theta_{x,m}$ between 0° and 360° is presented. The panels correspond to the (a) heavier current sheet approximation and (b) the lighter current sheet approximation from Figure 3. We evaluate the reconnection voltage assuming that the reconnection site forms at $\rho \sim 25 R_S$. In each panel, three black lines indicate: $\theta_x = 180^\circ$, the “theoretical limit” on the expected extent of the PPO-driven reconnection X-line; $\theta_x = 84^\circ$, a case study of an interval where reconnection is expected to be actively occurring; and 23° , the time-average angular extent of the X-line that accounts for the variability of the relative configuration and amplitudes of the PPO systems.

In Figure 7, we present the expected reconnection voltage over 1 PPO cycle for all iterations of $\theta_{x,m}$ between the exhaustive limits of 0° – 360° , assuming PPO-driven reconnection occurs in a (a) heavier and (b) lighter current sheet. We consider a fixed radial distance of $\rho \sim 25 R_S$, as it lies within the radial distance range ~ 20 – $30 R_S$ where the statistical X-line may form in Saturn’s magnetosphere (A. W. Smith et al., 2016). The voltages may vary by a few kV for reconnection sites at other radial distances, but this variability is not expected to be very large seeing as even though E decreases with radial distance, the length of the X-line associated with a fixed angular extent of PPO phases increases with radial distance.

On Figure 7, solid black lines indicate three values of θ_x : 180° which is the theoretical limit on the extent of the X-line, seeing as PPO phase angles $\Psi_{N/S}$ that are separated by $\sim 180^\circ$ are associated with opposing dynamics (i.e., $\Psi_N = 0^\circ$ is associated with thinning the equatorial current sheet, whereas $\Psi_N = 180^\circ$ is associated with thickening it); 23° , the time-averaged extent of reconnection favorable PPO phases evaluated in Section 3; and $\sim 84^\circ$, which is the average θ_x from the two data intervals presented in Figure 4 at $\Delta\Phi = 180^\circ$, calculated using the upper-quartile of the $D_{N/S}$ distributions constrained by A20/21. The final θ_x value is used as a proxy for a short-timescale, “Active Time Case Study”, since we know those conditions are statistically likely and favorable for PPO-driven reconnection.

In Figure 7, the reconnection voltages associated with PPO-driven reconnection on short-term timescales, that is, for $\theta_x \sim 84^\circ$ have an upper-limit in the range between (a) ~ 75 kV (heavier current sheet) and (b) ~ 325 kV (lighter current sheet) over 1 PPO cycle for $\theta_m = 180^\circ$. On longer-term timescales, we assume a more consistent $\theta_x \sim 23^\circ$, and the reconnection voltages over 1 PPO cycle lie in the range between (a) ~ 20 kV (heavier) and (b) ~ 100 kV (lighter).

The long-term reconnection voltages associated with Dungey- and Vasyliunas style reconnection are shown to be on the order of ~ 40 kV (Masters et al., 2014) and ~ 100 – 200 kV (Badman & Cowley, 2007), respectively. Although, on shorter timescales associated with intervals of solar wind compression, voltages associated with Dungey style reconnection are expected to reach ~ 100 kV (Badman & Cowley, 2007). During intervals of solar wind compression, that is, where Dungey style reconnection may be active, Provan et al. (2021) find a $\sim 15\%$ increase in the half-thickness of the nightside current sheet and Bradley et al. (2020) show an enhancement in reconnection signatures when the solar wind compressions are coincident with PPO dynamics expected to thin the equatorial current sheet (i.e., $\Delta\Phi \sim 180^\circ \pm 90^\circ$). While a thicker current sheet corresponds to conditions that are less favorable for PPO-driven reconnection, A20/21 suggest that intervals of significant solar wind compression might be accompanied by an enhancement in PPO amplitude. Although we cannot distinguish which of these two drivers controls reconnection dynamics in Saturn's magnetosphere, we speculate that the role of PPOs in driving reconnection is not expected to be diminished by the solar wind compressions Saturn's magnetosphere.

The short-term timescale voltage range of ~ 75 – 325 kV evaluated in our study for when PPO-driven reconnection is actively occurring shows that this phenomenon may be able to compete with, and perhaps even dominate over, the Vasyliunas cycle in Saturn's magnetosphere while it is actively occurring. Reconnection voltages with magnitudes of approximately a few hundred kV have previously been determined empirically by Arridge et al. (2016) and Jackman et al. (2011) over short-term timescales for tail reconnection events in Saturn's magnetosphere. However, on long-term timescales, where PPO-driven reconnection is not expected to be an ongoing process, the reconnection voltage range evaluated in our study is more comparable to the long-term Dungey Cycle estimates.

4.2. Mass Loss From the Magnetosphere

Indirect evidence of mass loss from Saturn's magnetosphere had been inferred from the bi-modal distribution of the size of Saturn's magnetopause by Achilleos et al. (2008), attributing some of the variability to mass loss events that were expected to last “several hours” and recur every ~ 5 – 10 days. Consequent studies by authors such as Hill et al. (2008) and Jackman et al. (2009) presented direct evidence of mass loss from the magnetosphere via the detection of plasmoids, which are loop-like structures enclosing magnetic flux and plasma that are expelled from the magnetosphere following magnetic reconnection. Observational predictions of plasmoid occurrence rates vary between ~ 1 per hr from specific case studies (Jackman & Arridge, 2011) to more statistically averaged values of ~ 5 per day (Garton et al., 2021; A. W. Smith et al., 2016) in Saturn's magnetosphere. Modeled predictions of plasmoid occurrence rates vary between ~ 1 every 7 min (for plasmoids of volume $\sim 10 R_S^3$ with mass density associated with 18 amu ions; Bagenal & Delamere, 2011), and ~ 1 per planetary rotation from MHD simulations of Saturn's magnetosphere driven by the polar-ionospheric flows which may drive PPOs (Jia & Kivelson, 2012).

For a fixed point in Saturn's magnetosphere where reconnection is favorable, a PPO X-line with $\theta_x = 23^\circ$ indicates the possibility of continuous reconnection occurring for ~ 40 min per PPO cycle. Assuming that the current sheet loses mass via plasmoid formation during this time, then the reconnection voltage associated with $\theta_m \sim 180^\circ$ would lie in the previously stated range of ~ 20 kV (heavier current sheet) and ~ 100 kV (lighter current sheet) over 1 PPO cycle.

Since we do not know the full spatial extent of the plasmoid structure that would form during such an event, we determine the expected mass loss from the magnetosphere by scaling our modeled rate of flux by the mass-per-unit magnetic flux of $\sim 10^{-3}$ kg/Wb determined by McAndrews et al. (2009) for Saturn's magnetosphere.

On short-term timescales, for example, our case study of $\theta_x \sim 84^\circ$, the modeled fluxes have an upper-limit in the range between ~ 0.9 and 4 GWb over 1 PPO cycle. This indicates mass loss rates that lie within the range ~ 75 – 325 kg/s. Provided that the current sheet is not significantly mass depleted for the majority of the event, the modeled mass loss rates are consistent with the short-term mass-loading rates of ~ 8 – 250 kg/s from Enceladus, determined by Bagenal and Delamere (2011).

On longer-term timescales, where $\theta_{x,m} = 23^\circ, 180^\circ$, the modeled fluxes lie in the range between ~ 0.4 and 2 GWb, which corresponds to mass loss rates in the range ~ 20 – 100 kg/s. The time-averaged mass-loading from Enceladus in the inner magnetosphere is expected to be on the order of ~ 100 kg/s, which indicates that at least $\sim 20\%$ of the mass loss from the magnetosphere could be attributed to PPO dynamics.

Since the angular extent of reconnection favorable PPO phases can vary with PPO modulation amplitude and beat phase, for smaller values of θ_x , we might expect the long term mass loss to occur in the form of small-scale “drizzle-like” reconnection in Saturn's magnetosphere, as predicted by authors such as Bagenal and Delamere (2011), Delamere et al. (2015), and Thomsen et al. (2014). Theoretical calculations of magnetodisc equilibria for the Jovian middle magnetosphere also suggest the possibility of drizzle-like plasma ejection following reconnection in that region (e.g., Nichols et al., 2015).

5. Conclusions

In this study, we set out to answer the following questions: could the PPO-driven thinning of Saturn's equatorial current sheet trigger the onset of magnetic reconnection under typical magnetospheric conditions? If so, what is the relative contribution of this phenomenon toward global magnetospheric circulation and mass loss at Saturn on both short- and long-term timescales?

Using empirical constraints on the PPO systems presented by Agiwal et al. (2021) and Agiwal et al. (2020) (A20/21) and an empirical model of PPO modulation of Saturn's equatorial current sheet (Cowley & Provan, 2017), we show that PPO-driven reconnection can in fact occur in Saturn's magnetosphere, but it is not expected to be an on-going process. We find that the onset of PPO-driven magnetic reconnection is dependent on the amplitude of modulation and beat phase of the PPO systems, which both vary with time, as well as spatial asymmetries in the current sheet half-thickness and characteristic ion kinetic length scales, which make PPO-driven reconnection more likely in the midnight and dawn local time sectors.

On short-term timescales, while PPO-driven reconnection is expected to be active, we evaluate reconnection voltages that have an upper-limit that lies in the range between ~ 75 – 325 kV on the order of 1 PPO cycle (~ 10.6 hr), which might consistently be applied to the magnetosphere for ~ 1 – 2 weeks every ~ 6 – 8 weeks. During these intervals, while PPO-driven reconnection is expected to be active, the mass loss rate associated with PPO-driven reconnection would lie in the range between ~ 75 – 325 kg/s, which is consistent with the short-term mass-loading rates of ~ 8 – 250 kg/s from Enceladus (Bagenal & Delamere, 2011).

However, taking into account the irregular nature of this phenomenon, we evaluate long-term reconnection voltages that lie in the range between ~ 20 – 100 kV on the order of 1 PPO cycle, that would consistently be applied to the magnetosphere on year-long timescales. The associated mass loss rates are estimated to lie in the range ~ 20 – 100 kg/s, which is consistent with the time-averaged mass-loading rate of ~ 100 kg/s from Enceladus (Bagenal & Delamere, 2011).

It is clear then that on long-term timescales, PPO-driven reconnection, where atmospheric perturbations drive large-scale thinning of the equatorial current sheet globally, is unlikely to be able to compete with the much more dominant Vasyliunas cycle, where equatorially mass-loaded field lines become radially distended in the post-dusk magnetosphere. The Vasyliunas cycle is expected to consistently drive which is expected to consistently drive the magnetosphere with voltages of ~ 100 – 200 kV, unless the PPO dynamics are constantly operating in a severely mass depleted current sheet (which is highly unlikely). However, while PPO-driven reconnection is

actively occurring, the reconnection voltages and mass loss associated with PPO dynamics may at times be on par with, if not more dominant than, co-rotation driven dynamics in Saturn's magnetosphere.

Data Availability Statement

Cassini magnetometer data supporting this work are publicly available on the Imperial College London MAGDA server (<https://magda.imperial.ac.uk/>) and the NASA Planetary Data System at the Jet Propulsion Laboratory (<https://pds.jpl.nasa.gov/>). The Cassini plasma moments used in this study are derived using the data products from Wilson et al. (2017).

Acknowledgments

O. Agiwal was supported by NASA under Grant No. 80NSSC21K0157 issued through the Solar System Workings Program and by STFC grant ST/R504816/1. G. J. Hunt was supported by STFC grant ST/N000692/1. A. Masters was supported by a Royal Society University Research Fellowship. M. K. Dougherty was funded by Royal Society Research Professorship RP140004.

References

- Achilleos, N., Arridge, C. S., Bertucci, C., Jackman, C. M., Dougherty, M. K., Khurana, K. K., & Russell, C. T. (2008). Large-scale dynamics of Saturn's magnetopause: Observations by Cassini. *Journal of Geophysical Research: Space Physics*, *113*(11). <https://doi.org/10.1029/2008JA013265>
- Agiwal, O. (2021). *Investigating temporally variable magnetospheric dynamics at Saturn (Doctoral dissertation)*. London: Imperial College London. <https://doi.org/10.25560/91910>
- Agiwal, O., Cao, H., Cowley, S. W. H., Dougherty, M. K., Hunt, G. J., Müller-Wodarg, I., & Achilleos, N. (2021). Constraining the temporal variability of neutral winds in Saturn's low-latitude ionosphere using magnetic field measurements. *Journal of Geophysical Research: Planets*, *126*, e2020JE006578. <https://doi.org/10.1029/2020je006578>
- Agiwal, O., Hunt, G. J., Dougherty, M. K., Cowley, S. W. H., & Provan, G. (2020). Modeling the temporal variability in Saturn's magnetotail current sheet from the cassini F-ring orbits. *Journal of Geophysical Research: Space Physics*, *125*(3), 2019JA027371. <https://doi.org/10.1029/2019JA027371>
- Andrews, D. J., Bunce, E. J., Cowley, S. W. H., Dougherty, M. K., Provan, G., & Southwood, D. J. (2008). Planetary period oscillations in Saturn's magnetosphere: Phase relation of equatorial magnetic field oscillations and Saturn kilometric radiation modulation. *Journal of Geophysical Research*, *113*(A9). <https://doi.org/10.1029/2007ja012937>
- Andrews, D. J., Coates, A. J., Cowley, S. W. H., Dougherty, M. K., Lamy, L., Provan, G., & Zarka, P. (2010). Magnetospheric period oscillations at Saturn: Comparison of equatorial and high-latitude magnetic field periods with north and south Saturn kilometric radiation periods. *Journal of Geophysical Research*, *115*(A12). <https://doi.org/10.1029/2010JA015666>
- Andrews, D. J., Cowley, S. W. H., Dougherty, M. K., Lamy, L., Provan, G., & Southwood, D. J. (2012). Planetary period oscillations in Saturn's magnetosphere: Evolution of magnetic oscillation properties from southern summer to post-equinox. *Journal of Geophysical Research: Space Physics*, *117*(A4). <https://doi.org/10.1029/2011ja017444>
- Arridge, C. S., Eastwood, J. P., Jackman, C. M., Poh, G. K., Slavin, J. A., Thomsen, M. F., et al. (2016). Cassini in situ observations of long-duration magnetic reconnection in Saturn's magnetotail. *Nature Physics*, *12*(3), 268–271. <https://doi.org/10.1038/nphys3565>
- Arridge, C. S., Kane, M., Sergis, N., Khurana, K. K., & Jackman, C. M. (2015). Sources of local time asymmetries in magnetodiscs. *Space Science Reviews*, *187*(1–4), 301–333. https://doi.org/10.1007/978-1-4939-3395-2_8
- Arridge, C. S., Russell, C. T., Khurana, K. K., Achilleos, N., André, N., Rymer, A. M., et al. (2007). Mass of Saturn's magnetodisc: Cassini observations. *Geophysical Research Letters*, *34*(9). <https://doi.org/10.1029/2006GL028921>
- Badman, S. V., Branduardi-Raymont, G., Galand, M., Sébastien, Hess, L. G., Krupp, N., et al. (2015). Auroral processes at the giant planets: Energy deposition, emission mechanisms, morphology, and spectra. *Space Science Reviews*, *187*, 99–179. <https://doi.org/10.1007/s11214-014-0042-x>
- Badman, S. V., & Cowley, S. W. (2007). Significance of Dungey-cycle flows in Jupiter's and Saturn's magnetospheres, and their identification on closed equatorial field lines. *Annales Geophysicae*, *25*(4), 941–951. <https://doi.org/10.5194/angeo-25-941-2007>
- Bagenal, F., & Delamere, P. A. (2011). Flow of mass and energy in the magnetospheres of Jupiter and Saturn. *Journal of Geophysical Research: Space Physics*, *116*(5), 5209. <https://doi.org/10.1029/2010JA016294>
- Biskamp, D., Schwarz, E., & Drake, J. F. (1997). Two-fluid theory of collisionless magnetic reconnection. *Physics of Plasmas*, *4*(4), 1002–1009. <https://doi.org/10.1063/1.872211>
- Bradley, T. J., Cowley, S. W., Bunce, E. J., Melin, H., Provan, G., Nichols, J. D., et al. (2020). Saturn's nightside dynamics during Cassini's F ring and proximal orbits: Response to solar wind and planetary period oscillation modulations. *Journal of Geophysical Research: Space Physics*, *125*(9), e2020JA027907. <https://doi.org/10.1029/2020JA027907>
- Bradley, T. J., Cowley, S. W., Bunce, E. J., Smith, A. W., Jackman, C. M., & Provan, G. (2018). Planetary period modulation of reconnection bursts in Saturn's magnetotail. *Journal of Geophysical Research: Space Physics*, *123*(11), 9476–9507. <https://doi.org/10.1029/2018JA025932>
- Carbary, J. F., Achilleos, N., & Arridge, C. S. (2012). Statistical ring current of Saturn. *Journal of Geophysical Research: Space Physics*, *117*(A6). <https://doi.org/10.1029/2011ja017472>
- Chen, Y., Tóth, G., Cassak, P., Jia, X., Gombosi, T. I., Slavin, J. A., et al. (2017). Global three-dimensional simulation of Earth's dayside reconnection using a two-way coupled magnetohydrodynamics with embedded particle-in-cell model: Initial results. *Journal of Geophysical Research: Space Physics*, *122*(10), 318–410. <https://doi.org/10.1002/2017JA024186>
- Chowdhury, M. N., Stallard, T. S., Baines, K. H., Provan, G., Melin, H., Hunt, G. J., et al. (2022). Saturn's weather-driven aurorae modulate oscillations in the magnetic field and radio emissions. *Geophysical Research Letters*, *49*(3), e2021GL096492. <https://doi.org/10.1029/2021gl096492>
- Connerney, J. E., Acuna, M. H., & Ness, N. F. (1983). Currents in Saturn's magnetosphere. *Journal of Geophysical Research*, *88*(A11), 8779–8789. <https://doi.org/10.1029/ja088ia11p08779>
- Cowley, S. W. H., & Provan, G. (2017). Planetary period modulations of Saturn's magnetotail current sheet during northern spring: Observations and modeling. *Journal of Geophysical Research: Space Physics*, *122*(6), 6049–6077. <https://doi.org/10.1002/2017JA023993>
- Cowley, S. W. H., & Provan, G. (2021). Physical origin of recurrent magnetic dipolarization events in Saturn's equatorial plasma sheet. *Journal of Geophysical Research: Space Physics*, *126*(8), e2021JA029444. <https://doi.org/10.1029/2021ja029444>
- Cowley, S. W. H., Provan, G., Hunt, G. J., & Jackman, C. M. (2017). Planetary period modulations of Saturn's magnetotail current sheet: A simple illustrative mathematical model. *Journal of Geophysical Research: Space Physics*, *122*, 258–279. <https://doi.org/10.1002/2016JA023367>
- Delamere, P. A., Otto, A., Ma, X., Bagenal, F., & Wilson, R. J. (2015). Magnetic flux circulation in the rotationally driven giant magnetospheres. *Journal of Geophysical Research: Space Physics*, *120*(6), 4229–4245. <https://doi.org/10.1002/2015JA021036>

- DiBraccio, G. A., Slavin, J. A., Boardsen, S. A., Anderson, B. J., Korth, H., Zurbuchen, T. H., et al. (2013). MESSENGER observations of magnetopause structure and dynamics at Mercury. *Journal of Geophysical Research: Space Physics*, *118*(3), 997–1008. <https://doi.org/10.1002/jgra.50123>
- Dougherty, M. K. (2006). Identification of a dynamic atmosphere at Enceladus with the Cassini magnetometer. *Science*, *311*(5766), 1406–1409. <https://doi.org/10.1126/science.1120985>
- Dougherty, M. K., Kellock, S., Southwood, D. J., Balogh, A., Smith, E. J., Tsurutani, B. T., et al. (2004). The Cassini magnetic field investigation. *Space Science Reviews*, *114*(1–4), 331–383. https://doi.org/10.1007/978-1-4020-2774-1_4
- Dungey, J. W. (1963). The effect of quasi-static electric fields on Van Allen particles. *Journal of Geophysical Research*, *68*(11), 3540–3541. <https://doi.org/10.1029/jz068i011p03540>
- Espinosa, S. A., & Dougherty, M. K. (2000). Unexpected periodic perturbations in Saturn's magnetic field data from pioneer 11 and voyager 2. *Geophysical Research Letters*, *27*(17), 2785–2788. <https://doi.org/10.1029/2000gl000048>
- Espinosa, S. A., Southwood, D. J., & Dougherty, M. K. (2003). How can Saturn impose its rotation period in a noncorotating magnetosphere? *Journal of Geophysical Research: Space Physics*, *108*(A2). <https://doi.org/10.1029/2001JA005084>
- Fuselier, S. A., Frahm, R., Lewis, W. S., Masters, A., Mukherjee, J., Petrinec, S. M., & Sillanpaa, I. J. (2014). The location of magnetic reconnection at Saturn's magnetopause: A comparison with Earth. *Journal of Geophysical Research: Space Physics*, *119*(4), 2563–2578. <https://doi.org/10.1002/2013JA019684>
- Garton, T. M., Jackman, C. M., Smith, A. W., Yeakel, K. L., Maloney, S. A., & VandeGriff, J. (2021). Machine learning applications to Kronian magnetospheric reconnection classification. *Frontiers in Astronomy and Space Sciences*, *7*, 104. <https://doi.org/10.3389/fspas.2020.600031>
- Giampieri, G. (2004). Rotation rate of Saturn's interior from magnetic field observations. *Geophysical Research Letters*, *31*(16), L16701. <https://doi.org/10.1029/2004gl020194>
- Hill, T. W., Thomsen, M. F., Henderson, M. G., Tokar, R. L., Coates, A. J., McAndrews, H. J., et al. (2008). Plasmoids in Saturn's magnetotail. *Journal of Geophysical Research: Space Physics*, *113*(1). <https://doi.org/10.1029/2007JA012626>
- Huddleston, D. E., Russell, C. T., Le, G., & Szabo, A. (1997). Magnetopause structure and the role of reconnection at the outer planets. *Journal of Geophysical Research: Space Physics*, *102*(A11), 24289–24302. <https://doi.org/10.1029/97JA02416>
- Hunt, G. J., Cowley, S. W., Provan, G., Bunce, E. J., Alexeev, I. I., Belenkaya, E. S., et al. (2014). Field-aligned currents in Saturn's southern nightside magnetosphere: Subcorotation and planetary period oscillation components. *Journal of Geophysical Research: Space Physics*, *119*, 9847–9899. <https://doi.org/10.1002/2014JA020506>
- Jackman, C. M., & Arridge, C. S. (2011). Statistical properties of the magnetic field in the Kronian magnetotail lobes and current sheet. *Journal of Geophysical Research: Space Physics*, *116*(A5). <https://doi.org/10.1029/2010ja015973>
- Jackman, C. M., Arridge, C. S., McAndrews, H. J., Henderson, M. G., & Wilson, R. J. (2009). Northward field excursions in Saturn's magnetotail and their relationship to magnetospheric periodicities. *Geophysical Research Letters*, *36*(16). <https://doi.org/10.1029/2009GL039149>
- Jackman, C. M., Provan, G., & Cowley, S. W. (2016). Reconnection events in Saturn's magnetotail: Dependence of plasmoid occurrence on planetary period oscillation phase. *Journal of Geophysical Research—A: Space Physics*, *121*(4), 2922–2934. <https://doi.org/10.1002/2015JA021985>
- Jackman, C. M., Slavin, J. A., & Cowley, S. W. H. (2011). Cassini observations of plasmoid structure and dynamics: Implications for the role of magnetic reconnection in magnetospheric circulation at Saturn. *Journal of Geophysical Research: Space Physics*, *116*(A10). <https://doi.org/10.1029/2011JA016682>
- Jackman, C. M., Slavin, J. A., Kivelson, M. G., Southwood, D. J., Achilleos, N., Thomsen, M. F., et al. (2014). Saturn's dynamic magnetotail: A comprehensive magnetic field and plasma survey of plasmoids and traveling compression regions and their role in global magnetospheric dynamics. *Journal of Geophysical Research: Space Physics*, *119*(7), 5465–5494. <https://doi.org/10.1002/2013JA019388>
- Jia, X., & Kivelson, M. G. (2012). Driving Saturn's magnetospheric periodicities from the upper atmosphere/ionosphere: Magnetotail response to dual sources. *Journal of Geophysical Research*, *117*(A11219). <https://doi.org/10.1029/2012JA018183>
- Jia, X., & Kivelson, M. G. (2016). Dawn-dusk asymmetries in rotating magnetospheres: Lessons from modeling Saturn. *Journal of Geophysical Research—A: Space Physics*, *121*(2), 1413–1424. <https://doi.org/10.1002/2015JA021950>
- Kellett, S., Arridge, C. S., Bunce, E. J., Coates, A. J., Cowley, S. W., Dougherty, M. K., et al. (2011). Saturn's ring current: Local time dependence and temporal variability. *Journal of Geophysical Research: Space Physics*, *116*(5). <https://doi.org/10.1029/2010ja016216>
- Kivelson, M. G., & Jia, X. (2014). Control of periodic variations in Saturn's magnetosphere by compressional waves. *Journal of Geophysical Research: Space Physics*, *119*(10), 8030–8045. <https://doi.org/10.1002/2014JA020258>
- Liu, Y. H., Kistler, L. M., Mouikis, C. G., Roytershteyn, V., & Karimabadi, H. (2014). The scale of the magnetotail reconnecting current sheet in the presence of O⁺. *Geophysical Research Letters*, *41*(14), 4819–4827. <https://doi.org/10.1002/2014GL060440>
- Mankovich, C., Marley, M. S., Fortney, J. J., & Movshovitz, N. (2019). Cassini ring seismology as a probe of Saturn's interior. I. Rigid rotation. *The Astrophysical Journal*, *871*(1), 1. <https://doi.org/10.3847/1538-4357/aaf798>
- Martin, C. J., & Arridge, C. S. (2017). Cassini observations of aperiodic waves on Saturn's magnetodisc. *Journal of Geophysical Research: Space Physics*, *122*(8), 8063–8077. <https://doi.org/10.1002/2017JA024293>
- Masters, A. (2015). The dayside reconnection voltage applied to Saturn's magnetosphere. *Geophysical Research Letters*, *42*(8), 2577–2585. <https://doi.org/10.1002/2015GL063361>
- Masters, A., Fujimoto, M., Hasegawa, H., Russell, C. T., Coates, A. J., & Dougherty, M. K. (2014). Can magnetopause reconnection drive Saturn's magnetosphere? *Geophysical Research Letters*, *41*(6), 1862–1868. <https://doi.org/10.1002/2014GL059288>
- McAndrews, H. J., Owen, C. J., Thomsen, M. F., Lavraud, B., Coates, A. J., Dougherty, M. K., & Young, D. T. (2008). Evidence for reconnection at Saturn's magnetopause. *Journal of Geophysical Research: Space Physics*, *113*(4). <https://doi.org/10.1029/2007JA012581>
- McAndrews, H. J., Thomsen, M. F., Arridge, C. S., Jackman, C. M., Wilson, R. J., Henderson, M. G., et al. (2009). Plasma in Saturn's nightside magnetosphere and the implications for global circulation. *Planetary and Space Science*, *57*(14–15), 1714–1722. <https://doi.org/10.1016/j.pss.2009.03.003>
- Morooka, M. W., Modolo, R., Wahlund, J. E., André, M., Eriksson, A. I., Persoon, A. M., et al. (2009). The electron density of Saturn's magnetosphere. *Annales Geophysicae*, *27*, 2971–2991. <https://doi.org/10.5194/angeo-27-2971-2009>
- Nakamura, T. K., Genestreti, K. J., Liu, Y. H., Nakamura, R., Teh, W. L., Hasegawa, H., et al. (2018). Measurement of the magnetic reconnection rate in the Earth's magnetotail. *Journal of Geophysical Research: Space Physics*, *123*(11), 9150–9168. <https://doi.org/10.1029/2018JA025713>
- Nichols, J. D., Achilleos, N., & Cowley, S. W. (2015). A model of force balance in Jupiter's magnetodisc including hot plasma pressure anisotropy. *Journal of Geophysical Research: Space Physics*, *120*(12), 10185–10206. <https://doi.org/10.1002/2015ja021807>
- Phan, T. D., Love, T. E., Gosling, J. T., Paschmann, G., Eastwood, J. P., Oieroset, M., et al. (2011). Triggering of magnetic reconnection in a magnetosheath current sheet due to compression against the magnetopause. *Geophysical Research Letters*, *38*(17). <https://doi.org/10.1029/2011GL048586>

- Provan, G., Andrews, D. J., Arridge, C. S., Coates, A. J., Cowley, S. W. H., Cox, G., et al. (2012). Dual periodicities in planetary-period magnetic field oscillations in Saturn's tail. *Journal of Geophysical Research: Space Physics*, 117(A1), 1–20. <https://doi.org/10.1029/2011ja017104>
- Provan, G., Andrews, D. J., Cecconi, B., Cowley, S. W. H., Dougherty, M. K., Lamy, L., & Zarka, P. M. (2011). Magnetospheric period magnetic field oscillations at Saturn: Equatorial phase “jitter” produced by superposition of southern and northern period oscillations. *Journal of Geophysical Research*, 116(A4). <https://doi.org/10.1029/2010JA016213>
- Provan, G., Bradley, T. J., Bunce, E. J., Cowley, S. W., Cao, H., Dougherty, M., et al. (2021). Saturn's nightside ring current during Cassini's grand finale. *Journal of Geophysical Research: Space Physics*, 126(3), e2020JA028605. <https://doi.org/10.1029/2020JA028605>
- Provan, G., Cowley, S. W., Lamy, L., Bunce, E. J., Hunt, G. J., Zarka, P., & Dougherty, M. K. (2016). Planetary period oscillations in Saturn's magnetosphere: Coalescence and reversal of northern and southern periods in late northern spring. *Journal of Geophysical Research: Space Physics*, 121, 9829–9862. <https://doi.org/10.1002/2016JA023056>
- Provan, G., Cowley, S. W. H., Bradley, T. J., Bunce, E. J., Hunt, G. J., & Dougherty, M. K. (2018). Planetary period oscillations in Saturn's magnetosphere: Cassini magnetic field observations over the northern summer solstice interval. *Journal of Geophysical Research: Space Physics*, 123(5), 3859–3899. <https://doi.org/10.1029/2018JA025237>
- Provan, G., Cowley, S. W. H., Sandhu, J., Andrews, D. J., & Dougherty, M. K. (2013). Planetary period magnetic field oscillations in Saturn's magnetosphere: Postequinox abrupt nonmonotonic transitions to northern system dominance. *Journal of Geophysical Research: Space Physics*, 118, 3243–3264. <https://doi.org/10.1002/jgra.50186>
- Reed, J. J., Jackman, C. M., Lamy, L., Kurth, W. S., & Whiter, D. K. (2018). Low-frequency extensions of the Saturn kilometric radiation as a proxy for magnetospheric dynamics. *Journal of Geophysical Research: Space Physics*, 123(1), 443–463. <https://doi.org/10.1002/2017JA024499>
- Sanny, J., McPherron, R. L., Russell, C. T., Baker, D. N., Pulkkinen, T. I., & Nishida, A. (1994). Growth-phase thinning of the near-Earth current sheet during the CDAW 6 substorm. *Journal of Geophysical Research: Space Physics*, 99(A4), 5805–5816. <https://doi.org/10.1029/93ja03235>
- Sergis, N., Arridge, C. S., Krimigis, S. M., Mitchell, D. G., Rymer, A. M., Hamilton, D. C., et al. (2011). Dynamics and seasonal variations in Saturn's magnetospheric plasma sheet, as measured by Cassini. *Journal of Geophysical Research: Space Physics*, 116(4). <https://doi.org/10.1029/2010JA016180>
- Sergis, N., Bunce, E. J., Carbary, J. F., Cowley, S. W., Jia, X., Hamilton, D. C., et al. (2018). The ring current of Saturn. In *Electric currents in geospace and beyond* (pp. 139–154). Wiley. <https://doi.org/10.1002/9781119324522.ch9>
- Sergis, N., Krimigis, S. M., Mitchell, D. G., Hamilton, D. C., Krupp, N., Mauk, B. M., et al. (2007). Ring current at Saturn: Energetic particle pressure in Saturn's equatorial magnetosphere measured with Cassini/MIMI. *Geophysical Research Letters*, 34(9). <https://doi.org/10.1029/2006GL029223>
- Sergis, N., Krimigis, S. M., Mitchell, D. G., Hamilton, D. C., Krupp, N., Mauk, B. H., et al. (2009). Energetic particle pressure in Saturn's magnetosphere measured with the magnetospheric Imaging instrument on cassini. *Journal of Geophysical Research: Space Physics*, 114(2). <https://doi.org/10.1029/2008JA013774>
- Sergis, N., Krimigis, S. M., Roelof, E. C., Arridge, C. S., Rymer, A. M., Mitchell, D. G., et al. (2010). Particle pressure, inertial force, and ring current density profiles in the magnetosphere of Saturn, based on Cassini measurements. *Geophysical Research Letters*, 37(2). <https://doi.org/10.1029/2009gl041920>
- Slavin, J. A., & Holzer, R. E. (1979). The effect of erosion on the solar wind stand-off distance at Mercury. *Journal of Geophysical Research*, 84(A5), 2076. <https://doi.org/10.1029/ja084ia05p02076>
- Smith, A. W., Jackman, C. M., & Thomsen, M. F. (2016). Magnetic reconnection in Saturn's magnetotail: A comprehensive magnetic field survey. *Journal of Geophysical Research—A: Space Physics*, 121(4), 2984–3005. <https://doi.org/10.1002/2015ja022005>
- Smith, C. G., & Achilleos, N. (2012). Axial symmetry breaking of Saturn's thermosphere. *Monthly Notices of the Royal Astronomical Society*, 422(2), 1460–1488. <https://doi.org/10.1111/j.1365-2966.2012.20719.x>
- Sorba, A. M., Achilleos, N. A., Sergis, N., Guio, P., Arridge, C. S., & Dougherty, M. K. (2019). Local time variation in the large-scale structure of Saturn's magnetosphere. *Journal of Geophysical Research: Space Physics*, 124(9), 7425–7441. <https://doi.org/10.1029/2018JA026363>
- Southwood, D. J., & Kivelson, M. G. (2007). Saturnian magnetospheric dynamics: Elucidation of a camshaft model. *Journal of Geophysical Research*, 112(A12222). <https://doi.org/10.1029/2007JA012254>
- Staniland, N. R., Dougherty, M. K., Masters, A., & Achilleos, N. (2021). The cushion region and dayside magnetodisc structure at Saturn. *Geophysical Research Letters*, 48(6), e2020GL091796. <https://doi.org/10.1029/2020GL091796>
- Staniland, N. R., Dougherty, M. K., Masters, A., & Bunce, E. J. (2020). Determining the nominal thickness and variability of the magnetodisc current sheet at Saturn. *Journal of Geophysical Research: Space Physics*, 125(5). <https://doi.org/10.1029/2020JA027794>
- Thomsen, M. F. (2013). Saturn's magnetospheric dynamics. *Geophysical Research Letters*, 40(20), 5337–5344. <https://doi.org/10.1002/2013GL057967>
- Thomsen, M. F., Jackman, C. M., Cowley, S. W., Jia, X., Kivelson, M. G., & Provan, G. (2017). Evidence for periodic variations in the thickness of Saturn's nightside plasma sheet. *Journal of Geophysical Research: Space Physics*, 122, 280–292. <https://doi.org/10.1002/2016JA023368>
- Thomsen, M. F., Jackman, C. M., Tokar, R. L., & Wilson, R. J. (2014). Plasma flows in Saturn's nightside magnetosphere. *Journal of Geophysical Research: Space Physics*, 119(6), 4521–4535. <https://doi.org/10.1002/2014JA019912>
- Tóth, G., Chen, Y., Gombosi, T. I., Cassak, P., Markidis, S., & Peng, I. B. (2017). Scaling the ion inertial length and its implications for modeling reconnection in global simulations. *Journal of Geophysical Research: Space Physics*, 122(10), 10336–10355. <https://doi.org/10.1002/2017JA024189>
- Vasyliunas, V. M. (1983). Plasma distribution and flow. In *Physics of the Jovian magnetosphere* (Vol. 12, pp. 395–453). Cambridge University Press. <https://doi.org/10.1017/cbo9780511564574.013>
- Wilson, R. J., Bagenal, F., & Persoon, A. M. (2017). Survey of thermal plasma ions in Saturn's magnetosphere utilizing a forward model. *Journal of Geophysical Research: Space Physics*, 122(7), 7256–7278. <https://doi.org/10.1002/2017JA024117>
- Yao, Z. H., Radioti, A., Grodent, D., Ray, L. C., Palmaerts, B., Sergis, N., et al. (2018). Recurrent magnetic dipolarization at Saturn: Revealed by Cassini. *Journal of Geophysical Research: Space Physics*, 123(10), 8502–8517. <https://doi.org/10.1029/2018JA025837>